Materials Research Bulletin 44 (2009) 1385–1391

Contents lists available at ScienceDirect

Materials Research Bulletin

journal homepage: www.elsevier.com/locate/matresbu

Inorganic–organic hybrid semiconductor nanomaterials: $(ZnSe)(N_2H_4)_x(C_5H_5N)_y$

Lina Liu [a], Hongwei Song [b,*], Libo Fan [a], Fang Wang [a], Ruifei Qin [a], Biao Dong [a], Haifeng Zhao [a], Xinguang Ren [a], Guohui Pan [a], Xue Bai [a], Qilin Dai [a]

[a] *Key Laboratory of Excited State Physics, Changchun Institute of Optics, Fine Mechanics and Physics, Chinese Academy of Sciences, and Graduate School of Chinese Academy of Sciences, 16 Eastern Nan-Hu Road, Changchun 130033, PR China*
[b] *State Key Laboratory of Integrated Optoelectronics, College of Electronic Sciences and Engineering, Jilin University, 2699 Qianjin Street, Changchun 130012, PR China*

ARTICLE INFO

Article history:
Received 1 June 2008
Received in revised form 12 November 2008
Accepted 27 November 2008
Available online 3 December 2008

Keywords:
A. Composites
B. Nanostructures
C. Semiconductors
D. Luminescence

ABSTRACT

In this paper, inorganic–organic hybrid semiconductor $(ZnSe)(N_2H_4)_x(C_5H_5N)_y$ nanosheets as well as $(ZnSe)(C_5H_5N)_y$ nanoparticles were first synthesized by a solvothermal method in a ternary solution and characterized by X-ray diffraction (XRD), scanning electron microscopy (SEM), Fourier transform infrared (FT-IR) spectra, ultraviolet–visible (UV–vis) absorption spectra, thermogravimetric analysis (TGA), differential scanning calorimeter (DSC) and photoluminescence (PL) spectra. The results indicated that the morphology and composition of the products were largely influenced by the reaction temperature and the volume ratio of water. When the reaction temperature and the water content were lower, $(ZnSe)(N_2H_4)_x(C_5H_5N)_y$ nanosheets were formed. As the reaction temperature or the content of water was high enough, $(ZnSe)(C_5H_5N)_y$ nanoparticles were formed. Pure hexagonal wurtzite ZnSe nanosheets or zinc blende ZnSe nanoparticles were obtained by extracting the corresponding hybrids. The bandgap absorption of ZnSe nanocrystals blue shifted in comparison with the bulk. The photoluminescent intensity of $(ZnSe)(N_2H_4)_x(C_5H_5N)_y$ nanosheets was much stronger than that of $(ZnSe)(C_5H_5N)_y$ nanoparticles.

1. Introduction

Semiconductor nanomaterials have attracted considerable attention due to their unique properties [1–3] since quantum confinement effects were observed in 1980s. In contrast to the bulk materials, these nanomaterials have a large surface to volume ratio and exhibit size-dependent physical and chemical properties such as a blue-shift of absorption onset, a change of electrochemical potential of band edge, and an enhancement of photocatalytic activities with decreasing crystallite size [4]. Among them, as an important II–VI semiconductor, ZnSe has a wide band gap (~2.67 eV), high luminescent efficiency, low absorption coefficient and excellent transparency in infrared range [4–6], so it has been considered as a prospective material for the fabrication of optoelectronic devices, such as blue–green laser diodes and tunable mid-IR laser sources [7]. Besides, ZnSe also has potential applications in optically controlled switching due to its giant photoresistivity [8].

The combination of inorganic semiconductor with organic substance endows the resulted nanocomposites with good processability and improved physical, mechanical, and electrical properties such as enhanced solubility, conductivity, magnetic and optoelectronic properties and these nanocomposities have drawn considerable attention recently [9–13]. This kind of inorganic–organic hybrids are most desirable for low-weight and flexible photovoltaic devices. The hybrids of ZnSe with organic substance, for example, $ZnSe/N_2H_4$ nanosheets (NSs) [18], have been prepared [14–19]. In this work, we report a simple solvothermal route for the preparation of inorganic–organic hybrid $(ZnSe)(N_2H_4)_x(C_5H_5N)_y$ NSs as well as $(ZnSe)(C_5H_5N)_y$ nanoparticles (NPs). The shape and structure were easily controlled and some novel physical properties were obtained in the complicated hybrids. Pure hexagonal wurtzite ZnSe NSs and zinc blende ZnSe NPs were also obtained by extracting corresponding hybrids with ethylene glycol (EG).

2. Experimental

2.1. Sample preparation

In the preparation, the starting materials $Zn(CH_3COO)_2\cdot 2H_2O$, $N_2H_4\cdot H_2O$, C_5H_5N and $HOCH_2CH_2OH$ were all analytical grade and used without further purification. The purity of selenium (Alfa) was 99.999%. In a typical synthesis, 2 mmol $Zn(CH_3COO)_2\cdot 2H_2O$ and 2 mmol selenium were placed in a 50-mL Teflon-lined

---

* Corresponding author. Tel.: +86 431 86176320; fax: +86 431 86176320.
E-mail address: hwsong2005@yahoo.com.cn (H. Song).

0025-5408/$ – see front matter © 2008 Elsevier Ltd. All rights reserved.
doi:10.1016/j.materresbull.2008.11.023

stainless steel autoclave. Then the autoclave was filled with a mixture of C_5H_5N, $N_2H_4{\cdot}H_2O$ and water with a volume ratio of 25:5:1. The autoclave was sealed and maintained at 140 °C for 20 h in an oven. After the autoclave was cooled to room temperature naturally, the product was collected and washed with deionized water and absolute alcohol for several times and finally dried in vacuum at 80 °C for 4 h, which was labelled as sample A. By changing reaction conditions such as the reaction temperature, the reaction time and the volume ratio of C_5H_5N, $N_2H_4{\cdot}H_2O$ and water, samples B–H were obtained. The preparation processes for the other samples were nearly the same as that of sample A, except some detailed conditions. In the preparation of samples B, C and D, the volume ratios of C_5H_5N, $N_2H_4{\cdot}H_2O$ and water were 25:5:3, 25:5:5 and 25:5:12, respectively. In the preparation of samples E, F and G, the volume ratio of C_5H_5N, $N_2H_4{\cdot}H_2O$ and water was maintained at 25:5:3, and the reaction temperatures were changed, to be 120, 160 and 170 °C, respectively. In the preparation of sample H, the volume ratio of C_5H_5N, $N_2H_4{\cdot}H_2O$ and water was 25:5:3 and the reaction time were 40 h. To get pure ZnSe, half of sample B was placed in a 50-mL autoclave and the autoclave was filled with 35 mL ethylene glycol. Then the autoclave was sealed and maintained at 200 °C for 48 h in an oven. After the autoclave was cooled to room temperature naturally, the product was washed and dried just like sample B, which was labelled as sample I. Sample J was the product extracted from sample D using the same method. In comparison, the detailed reaction conditions of samples A–J were listed in Table 1. In the preparation of samples N30, N25, N20, N15 and N10, the reaction temperature was 160 °C and the volume ratios of $N_2H_4{\cdot}H_2O$, C_5H_5N and water were 30:0:0, 25:5:0, 20:10:0, 15:15:0 and 10:20:0, respectively.

2.2. Measurements

The data of X-ray diffraction (XRD) patterns were obtained on a Rigaku D/Max-Ra X-ray diffractometer using a Cu target radiation source (λ = 1.5418 Å). Field-emission scanning electron microscopy (FE-SEM) images were measured on a Hitachi S-4800 microscope. The transmission electron microscopy (TEM) image and the selected-area election diffraction (SAED) pattern were obtained with a JEM-2010 transmission election microscope made by Japanese JEOL Company. The Fourier transform infrared spectra (FT-IR) were recorded on a Bio-Rad FTS-3000 (EXCALIBUR SERIES) spectrometer. The powder samples were dispersed in absolute ethanol by ultrasonic to form a uniform suspension for the measurements of the UV–vis absorption spectra, which were performed on an UV-3101PC UV–VIS–NIR scanning spectrophotometer (SHIMADZU) at room temperature. Thermogravimetric analysis (TGA) and differential scanning calorimeter (DSC) were performed up to 1000 °C at a heating rate of 10 °C/min in a flowing nitrogen atmosphere on a PerkinElmer Pyris Diamond thermo-gravimetric analyzer. Emission spectra were taken at room temperature using a 325-nm He–Cd laser as the excitation source.

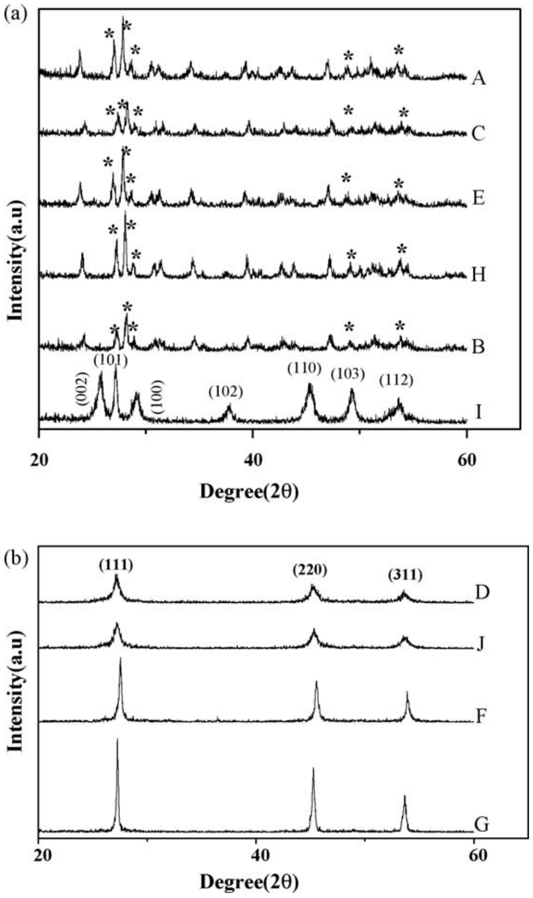

Fig. 1. XRD patterns of samples A–J: (A) sample A, (B) sample B, (C) sample C, (D) sample D, (E) sample E, (F) sample F, (G) sample G, (H) sample H, (I) sample I, (J) sample J. The diffraction peaks of hexagonal wurtzite ZnSe in samples A, B, C, E, H were labelled with asterisks (*).

3. Results and discussion

3.1. XRD patterns

The XRD patterns of various samples are depicted in Fig. 1. As can be seen from Fig. 1a, samples A, B, C, E and H have almost the same XRD pattern, indicating that they have the same crystal structure. Most of the XRD peaks cannot be indexed to any known phase of Zn, Se, ZnSe or ZnO provided in the standard JCPDS cards. These peaks may come from the crystalline organic materials. Similar results were also observed in other inorganic–organic composites [14,15,18,20–22]. The authors found that the XRD data exhibited great similarity with the theoretical XRD pattern of these inorganic–organic composites and conjectured that the samples

Table 1
A list of the reaction conditions, composition and morphology of different samples.

Sample	$VC_5H_5N/VN_2H_4{\cdot}H_2O/VH_2O$	Temperature (°C)	Time (h)	Composition	Morphology
A	25:5:1	140	20	$(ZnSe)(N_2H_4)_{0.83}\ (C_5H_5N)_{1.74}$	Short NSs
B	25:5:3	140	20	$(ZnSe)(N_2H_4)_{1.03}\ (C_5H_5N)_{1.79}$	Long NSs
C	25:5:5	140	20	$(ZnSe)(N_2H_4)_{0.85}\ (C_5H_5N)_{1.66}$	Fractal NSs
D	25:5:12	140	20	$(ZnSe)(C_5H_5N)_{1.64}$	NPs
E	25:5:3	120	20	$(ZnSe)(N_2H_4)_x\ (C_5H_5N)_y$	Short and Fractal NSs
F	25:5:3	160	20	$(ZnSe)(C_5H_5N)_y$	NWs and NPs
G	25:5:3	170	20	$(ZnSe)(C_5H_5N)_y$	Large particles
H	25:5:3	140	40	$(ZnSe)(N_2H_4)_x\ (C_5H_5N)_y$	Short NSs
I (extracted from sample B)	25:5:3	200	48	ZnSe	NSs
J (extracted from sample D)	25:5:12	200	48	ZnSe	NPs

had the lamellar structure with ZnSe nanolayers ordered via bridging N_2H_4 spacers. From Fig. 1a we can also observe the peaks coming from hexagonal wurtzite ZnSe in the samples, as labelled with asterisks, indicating that ZnSe exists in hybrid samples A, B, C, E and H. Sample I is pure ZnSe extracted from sample B. The XRD pattern of sample I indicates that sample I adopts the hexagonal wurtzite structure with lattice constants of $a = 4.000$ Å and $c = 6.552$ Å, which agrees well with the reported data (JCPDS card no. 15-0105). The detailed origins of the XRD peaks for sample I are labelled in the figure. The especially narrower width at the (0 0 2) face implies that the preferential growth is along the (0 0 2) face. In samples A, B, C, E and H, the diffraction peaks of (1 0 0), (0 0 2) and (1 0 1) planes have some shifts in comparison with sample I. According to Fig. 1b, the structure of samples D, J, F and G can be indexed to zinc blende ZnSe. Sample J is pure ZnSe extracted from sample D. In the XRD pattern of sample J, all reflection peaks can be readily indexed to zinc blende ZnSe (JCPDS card no. 05-0522) with the lattice constant $a = 5.663$ Å. Estimated using Scherrer's equation, the average crystallite size of sample J is about 15 nm. From the following analysis, we can know that samples A, B, C, E and H all consist of ZnSe, N_2H_4 and C_5H_5N, but samples D, F and G only consist of ZnSe and C_5H_5N. N_2H_4 may influence the crystal structure of ZnSe, so the XRD patterns of samples A, B, C, E and H cannot be indexed to the pure phase of ZnSe.

3.2. SEM and TEM images

Fig. 2 shows the SEM images of the inorganic–organic hybrids prepared at different reaction conditions. The size of NSs was measured from the separated ones. According to Fig. 2A(a)–(d), sample A yields NSs with a length of 300–500 nm and a width of ~200 nm. Sample B yields relatively uniform NSs with a length of 1–1.36 μm and a width of ~170 nm. Sample C mainly consists of fractal NSs. The thickness of these NSs is ~60 nm. Sample D yields NPs with a diameter of ~15 nm. Based on SEM images of samples A–D and detailed experimental conditions listed in Table 1, we can conclude that the morphology of the products is strongly influenced by the volume ratio of water. As the volume of water increased and the other conditions were maintained, the morphology of the products changed from NSs to NPs. Yadong Li and co-workers synthesized $ZnSe(N_2H_4)_x$ NSs using N_2H_4 as solvent and ZnSe NPs using water as solvent [18,23]. Our results also supported the conclusion that N_2H_4 was favorable to the formation of NSs and water was favorable to the formation of NPs.

As the reaction temperature varied, the morphology of the products also changed (see SEM images of samples B, E, F and G and Table 1). Sample B yields relatively uniform NSs. Sample E yields fractals with only a few uniform NSs. Sample F is a mixture of nanowires and NPs and sample G yields particles with a average diameter of 200 nm. In summary, when the volume ratio of C_5H_5N, $N_2H_4{\cdot}H_2O$ and water was 25:5:3, the reaction hardly took place if the temperature was lower than 100 °C. NSs were obtained in the temperature range of 100–140 °C. 140 °C was the optimal temperature for the formation of uniform NSs. When the temperature was higher than 140 °C, only particles or a mixture of nanowires and NPs were obtained. By comparing the SEM images of samples B and H (Fig. 2A(b) and (h)), it can be concluded that suitable reaction time is also important for the formation of

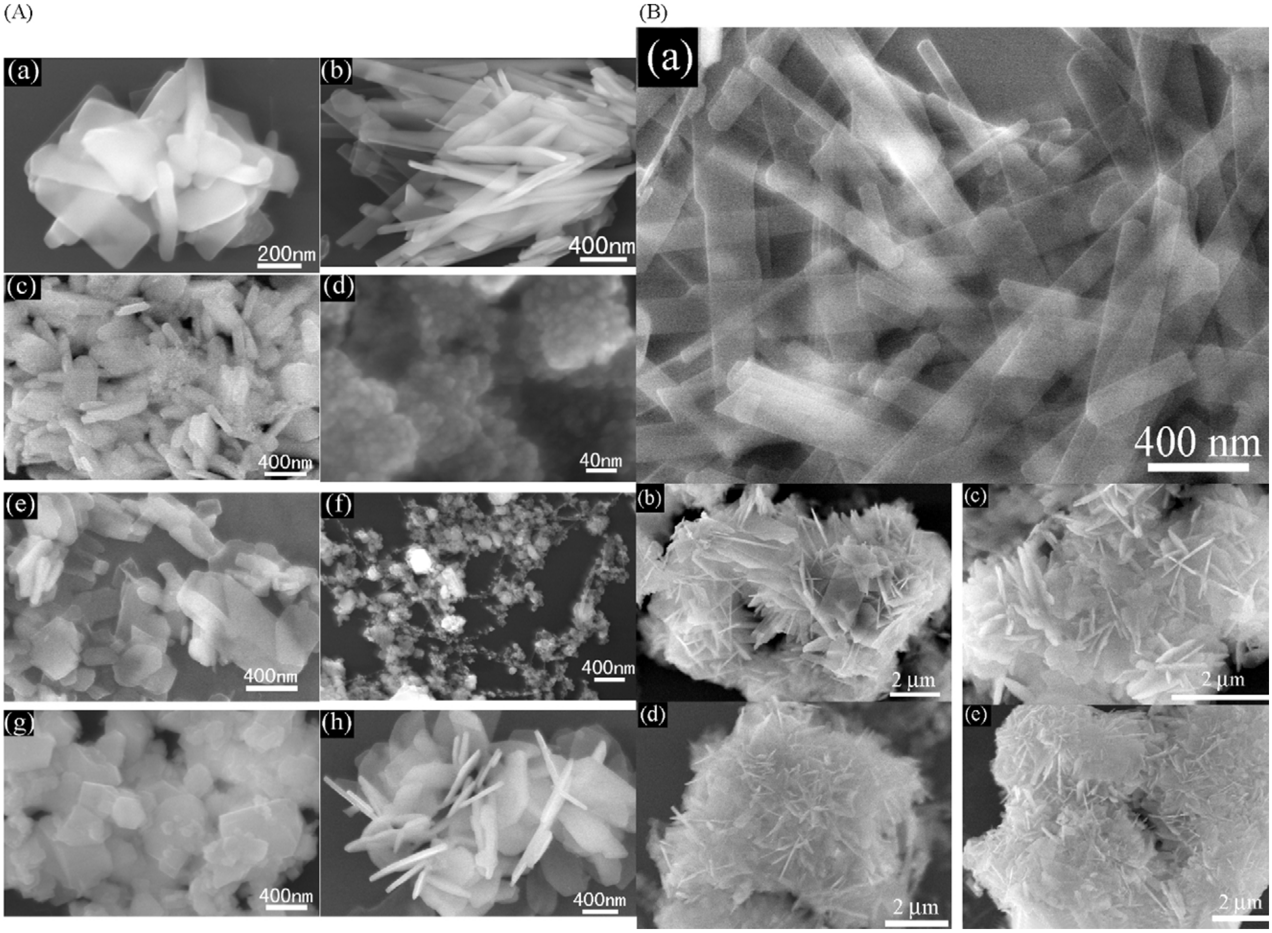

Fig. 2. (A) SEM images of (a) sample A, (b) sample B, (c) sample C, (d) sample D, (e) sample E, (f) sample F, (g) sample G, (h) sample H. (B) SEM images of (a) sample N30, (b) sample N25, (c) sample N20, (d) sample N15, (e) sample N10.

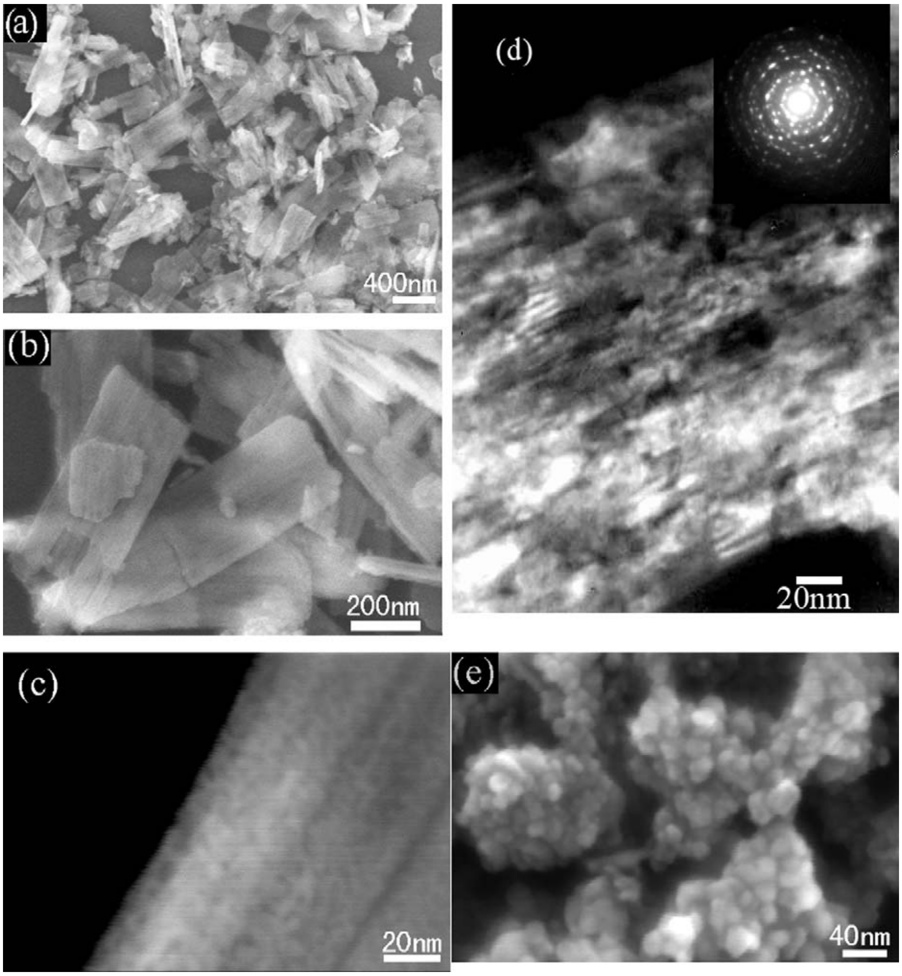

Fig. 3. SEM images of (a), (b), (c) sample I, TEM images of (d) sample I and SEM image of (e) sample J. The inset of image (d) is the SAED pattern of sample I.

uniform NSs. Higher temperature and pressure in the autoclave might destroy the uniform NSs and result in shorter NSs when the reaction continued for 40 h. In order to clarify whether the different volume ratios of C_5H_5N and $N_2H_4{\cdot}H_2O$ affect the morphology, samples N30, N25, N20, N15, N10 were prepared and the SEM images of them are shown in Fig. 2B. Uniform $ZnSe(N_2H_4)_x$ nanobelts were synthesized when pure $N_2H_4{\cdot}H_2O$ was used as solvent, which was consistent with other literatures [14,18]. When C_5H_5N was added to the reaction system, the nanobelts were clustered into groups, as shown in Fig. 2B(b)–(e). The morphology of the products was almost not affected by different volume ratios of C_5H_5N and $N_2H_4{\cdot}H_2O$.

Fig. 3 shows the SEM and TEM images of pure ZnSe extracted from the inorganic–organic hybrid nanomaterials. Fig. 3a–d indicates that sample I yields NSs, but the surface of the NSs is not as smooth as that of sample B. SAED pattern of sample I shown in the inset of Fig. 3d indicates that sample I is polycrystalline. Sample J was extracted from sample D. From Fig. 3e we can see that sample J yields NPs with a diameter of about 15 nm, which does not change in comparison with sample D. The morphology of samples A–J is listed in Table 1.

3.3. FT-IR spectra

FT-IR spectra of samples A–J are shown in Fig. 4. The IR spectra of samples A, B, C, E and H exhibit vibration bands corresponding to N_2H_4 molecules [24], suggesting that N_2H_4 exists in these samples. Two sharp peaks at 3112 and 3207 cm^{-1} are assigned to the N-H stretching vibration. The NH_2 scissors and twist bands appear at 1585 and 1154 cm^{-1}, respectively. In the IR spectra of samples D, F and G, vibration bands corresponding to N_2H_4 molecules do not appear, implying that samples D, F and G do not contain N_2H_4. Sample D was prepared with a higher volume ratio of water

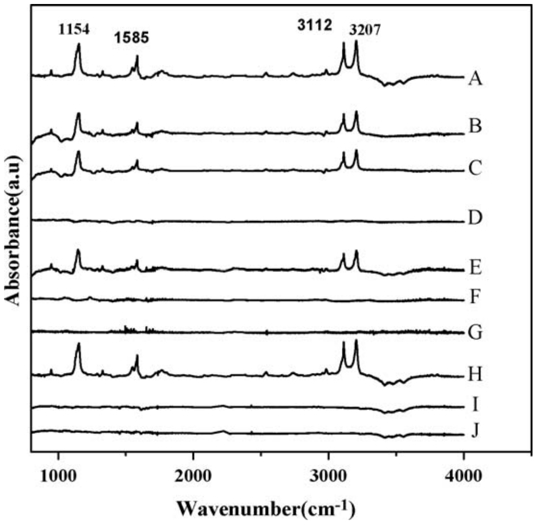

Fig. 4. FT-IR spectra of samples A–J: (A) sample A, (B) sample B, (C) sample C, (D) sample D, (E) sample E, (F) sample F, (G) sample G, (H) sample H, (I) sample I, (J) sample J.

(Table 1). Samples F and G were prepared at a higher temperature (160 and 170 °C). Accordingly, it can be concluded that N_2H_4 can only be achieved with a lower volume ratio of water and at a lower temperature. The reason for this will be discussed later. The vibration bands corresponding to N_2H_4 do not appear in the IR spectra of samples I and J, suggesting that N_2H_4 has been eliminated by extracting.

3.4. UV–vis absorption spectra

Fig. 5 shows UV–vis absorption spectra of samples A–J in contrast to C_5H_5N and N_2H_4. The samples A–H show a peak at 256 nm, which is the characteristic absorption of C_5H_5N, suggesting that samples A–H contain C_5H_5N. The absorption spectrum of $N_2H_4{\cdot}H_2O$ shows a broad and weak peak around 274 nm (Fig. 5b), which is too near to the absorption peak of C_5H_5N to determine the existence of $N_2H_4{\cdot}H_2O$ in samples A–H. The structure of our samples is very similar to those synthesized in other literatures [14,15,18,20,22]. There exists subnanometer structure formed by an interlaced arrangement of ZnSe and $N_2H_4{\cdot}H_2O$ or C_5H_5N [14,15,18,20]. Moreover, the thickness of ZnSe layers in the subnanometer structure is about several nanometers, and the diameter of the Bohr exciton in bulk ZnSe is on the order of 9 nm [25–27]. As a consequence, strong quantum confinement effect occurs in the ZnSe precursor, which leads the bandgap absorption of ZnSe to shift to 300 nm [14,15]. The absorption of C_5H_5N in ZnSe precursor (around 256 nm) is strong and close to 300 nm, so the bandgap absorption of ZnSe might be covered in samples A–H. The absorption spectra of sample A and C_5H_5N are magnified in Fig. 5c. An absorption band around 304 nm is observed in sample A, which largely blue shifts in comparison with that of bulk ZnSe (464 nm) [28]. In samples I and J, the peak at 256 nm does not appear, suggesting that C_5H_5N was eliminated by EG from samples B and D. Combining the IR spectra of samples I and J, we can draw the conclusion that samples I and J are pure ZnSe. The composition of all samples can be determined from the IR spectra, UV–vis absorption spectra and the following DSC-TGA analysis, as listed in Table 1. Fig. 5b indicates that the bandgap absorption of ZnSe in samples I and J locates at 441 nm and 443 nm, respectively, which slightly blue shifts compared with that of bulk ZnSe. The subnanometer structure would collapse upon the removal of the organic spacers. The slight shift of the bandgap absorption may be caused by the exterior size effect and may be attributed to the weak quantum confinement of ZnSe nanocrystallites [29].

3.5. TGA–DSC analyses

To determine the thermal stabilization of the inorganic–organic hybrid nanomaterials and the content of organic substance in different samples, TGA and DSC analyses were performed. As shown in Fig. 6a and b, the TGA curves of samples A, B and C are very similar. They are all stable below 300 °C. When the temperature increases, they all exhibit two steps of weight loss. The first step corresponds to the loss of N_2H_4, while the second step

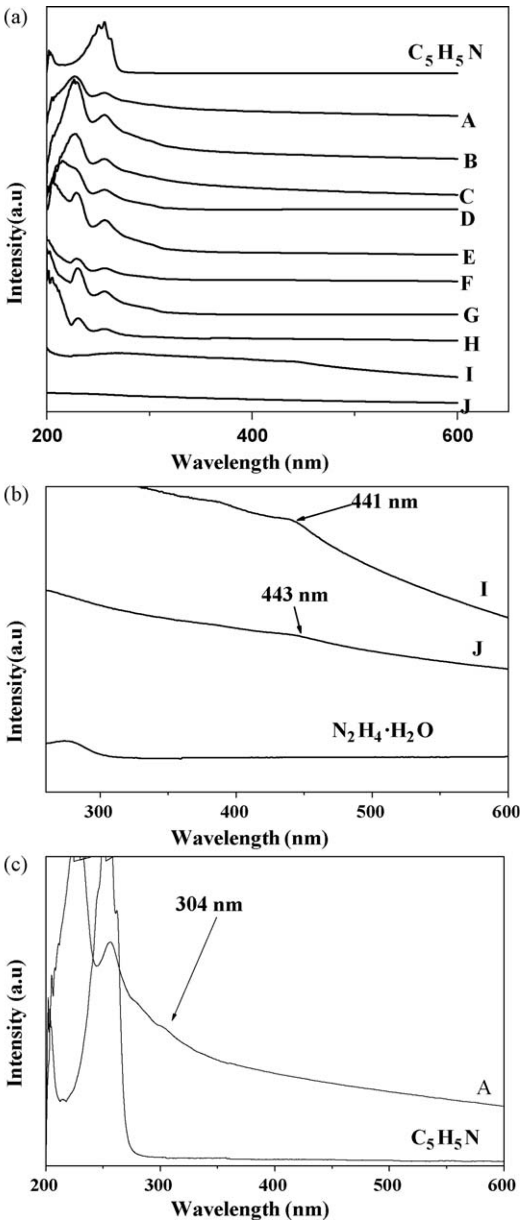

Fig. 5. (a) UV–vis absorption spectra of pyridine and various samples: (A) sample A, (B) sample B, (C) sample C, (D) sample D, (E) sample E, (F) sample F, (G) sample G, (H) sample H, (I) sample I, (J) sample J. (b) UV–vis absorption spectra of Hydrazine, (I) sample I and (J) sample J. (c) amplificatory UV–vis absorption spectra of (A) sample A and C_5H_5N.

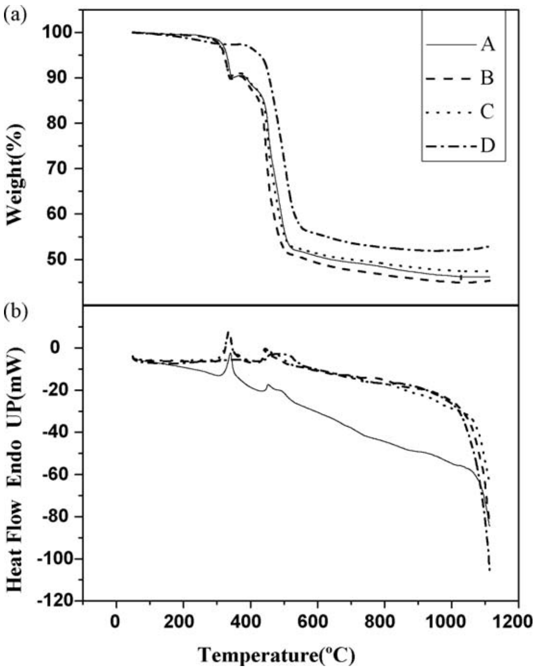

Fig. 6. The TGA and DSC curves of samples A, B, C, and D: (A) sample A, (B) sample B, (C) sample C and (D) sample D.

corresponds to the loss of C_5H_5N. The loss of N_2H_4 begins at 300 °C and ends at 340 °C. The loss of C_5H_5N begins at 380 °C and ends around 530 °C. However, sample D is stable below 390 °C and it contains only one organic substance, so the TGA curve of sample D exhibits one-step weight loss corresponding to the loss of C_5H_5N. The loss of C_5H_5N begins at 390 °C and ends around 560 °C, which defers in comparison with samples A, B and C. We can see that there is also a very small weight loss below 300 °C for all the four samples. It was attributed to the loss of water adsorbing on the surface of samples.

There are endothermic peaks at 340 and 450 °C corresponding to the loss of N_2H_4 and C_5H_5N in the DSC curves of samples A, B and C. There is only an endothermic peak around 500 °C, corresponding to the loss of C_5H_5N in the DSC curve of sample D. The content of N_2H_4 and C_5H_5N in samples A, B, C and D is listed in Table 1.

3.6. Possible formation mechanism

On the basis of above experimental results, the volume ratio of water, the reaction temperature and the reaction time all influence the crystal phase, morphology and composition of products. $(ZnSe)(N_2H_4)_x(C_5H_5N)_y$ NSs were obtained at a lower temperature and with a lower volume ratio of water (samples A, B, C, E and H). Extracting one of these samples produced pure hexagonal wurtzite ZnSe. On the contrary, $(ZnSe)(C_5H_5N)_y$ NPs were obtained at a higher temperature or with a higher volume ratio of water. Extracting one of these samples produced pure zinc blende ZnSe. This ternary-solution reaction is quite complicated, and the detailed mechanism needs to be resolved further. On the basis of the above experimental results, we propose a possible formation mechanism in the following. When the volume ratio of water and temperature is lower, the precursor can be formulated by the following equations [17]:

$$Zn^{2+} + xN_2H_4 + yC_5H_5N \rightarrow [Zn(N_2H_4)_x(C_5H_5N)_y]^{2+}, \tag{1}$$

$$2Se + N_2H_4 \rightarrow 2Se^{2-} + N_2 + 4H^+, \tag{2}$$

$$[Zn(N_2H_4)_x(C_5H_5N)_y]^{2+} + Se^{2-} \rightarrow ZnSe(N_2H_4)_x(C_5H_5N)_y. \tag{3}$$

Under this condition, the relative content of $N_2H_4{\cdot}H_2O$ is dominant in the ternary solution. $N_2H_4{\cdot}H_2O$ possibly combines with Zn^{2+} in a line owing to its linear structure, which not only greatly reduces the concentration of free Zn^{2+} in the solution, but also influences the growth of some planes, so that the reaction may proceed more slowly, providing enough time for the anisotropic growth of the samples. Furthermore, Deng and co-workers explained that there might be an energy-favorable route for the formation of hexagonal wurtzite structure when diamine solvents were used [20]. It is not hard to draw the conclusion that $N_2H_4{\cdot}H_2O$ supports the formation of NSs and that of hexagonal wurtzite ZnSe. The schematic illustration of the possible mechanism for the formation of the $(ZnSe)(N_2H_4)_x(C_5H_5N)_y$ NSs is drawn in Fig. 7. In the ternary solution, $N_2H_4{\cdot}H_2O$ could form a great number of reverse micelles as shown in the figure. Coordinate bonds formed between N atoms of $N_2H_4{\cdot}H_2O$ and Zn^{2+} inside the reverse micelles. Then Se^{2-} coming from the reaction of Se simple substance and N_2H_4 reacted with Zn^{2+}, which had coordinated with $N_2H_4{\cdot}H_2O$. The nuclei of ZnSe grew gradually and formed $(ZnSe)(N_2H_4)_x(C_5H_5N)_y$ NSs. After extracting, pure ZnSe nanosheets were obtained. Keeping the volume ratio of water unchanged and raising the temperature, the coordination bond between N_2H_4 and Zn^{2+} could not be formed. When the volume ratio of water was higher and the relative content of $N_2H_4{\cdot}H_2O$ was lower, water and C_5H_5N played a primary role in the formation of the products. Both water and C_5H_5N have no linear structure like $N_2H_4{\cdot}H_2O$, and they support the formation of particles and zinc blende ZnSe [19,23]. Only $(ZnSe)(C_5H_5N)_y$ NPs can be obtained. The solvent played a crucial role in controlling the morphology of the products, but the reaction temperature, reaction time, the coordinating ability of metal ions with the solvent, the concentration of solvent and metal ions all could influence the morphology of the products. Usually CdS nanorods were synthesized when ethylenediamine was added into the reaction system [30–32]. However, usually ZnE (E = S, Se) NSs were formed when the same solvent, ethylenediamine, was used [22,33,34]. We believe that this difference could be related to the difference in the coordinating ability of Cd^{2+} ions and Zn^{2+} ions with ethylenediamine (log β of $[Zn(en)_3]^{2+}$ and $[Cd(en)_3]^{2+}$ are 14.11 and 12.18, respectively). ZnS NPs and nanorods could be also prepared in ethylenediamine by changing the concentrations of ethylenediamine and metal ions, the reaction temperature and so on [35]. So we concluded that NSs, nanorods and NPs could be obtained by adding the same solvent, ethylenediamine. Likewise, the products with different morphologies could be also obtained by adding N_2H_4 in the reaction system [6,18,36]. Our results were consistent with these references (Table 1 and Fig. 2).

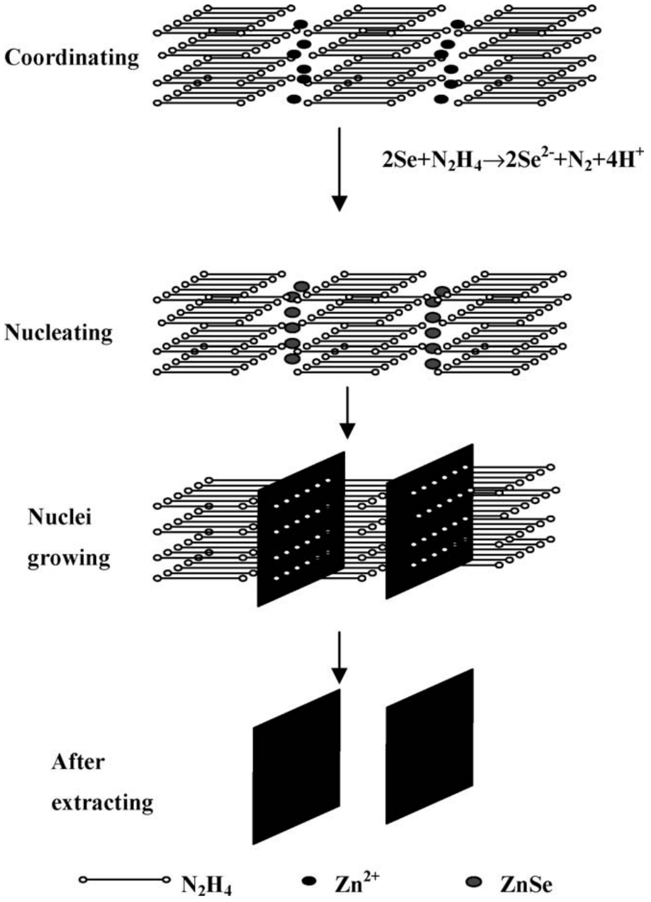

Fig. 7. Schematic illustration of a possible mechanism for the formation of $(ZnSe)(N_2H_4)_x(C_5H_5N)_y$ NSs.

3.7. Photoluminescence

The luminescent spectra of samples B, I, D and J which were measured under same conditions are shown in Fig. 8. Sample B shows an emission peak at about 615 nm, which associates with Zn vacancies in ZnSe [37,38]. Sample I shows two emission peaks. The emission peak around 466 nm is attributed to the near band edge (NBE) emission, which shifts red in comparison with the absorption spectrum due to Stokes effect [32,6], but it almost does not shift compared with bulk ZnSe. Compared with the blue-

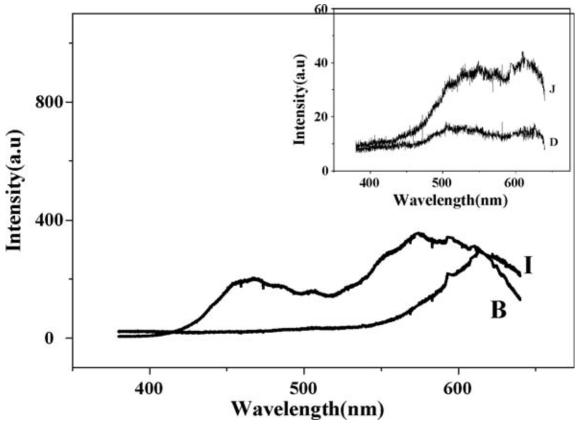

Fig. 8. Photoluminescent spectra of (B) sample B, (I) sample I, (D) sample D and (J) sample J with an excitation wavelength at 325 nm.

shift in the absorption spectrum of sample I, "Stokes effect" is dominant. The peak at 587 nm is attributed to self-activated luminescence, possibly due to donor-deep-acceptor pairs related to zinc vacancies and interstitial sites [17]. The combination of the near band edge emission and the self-activated luminescence gives a white-light emission, which may be used in the white-light emitting device. The PL spectra of sample D and sample J are shown in the inset of Fig. 8. Sample D shows two peaks at 613 and 550 nm, respectively. Sample J also shows two peaks, locating at 613 and 521 nm, respectively. These emission peaks are all the defect emissions in ZnSe. The peak at 613 nm is attributed to vacancies of Zn in ZnSe [30]. The emission peaks at 550 nm in sample D and 521 nm in sample J are other defect emissions of ZnSe [39]. We can see that most of the PL bands of samples B, I, D and J are from defects. The reason for this may be the nonstoichiometric ratio of Zn^{2+} and Se^{2-}. The EDAX data of these samples are not shown here. The number of Se^{2-} is larger than that of Zn^{2+} in these four samples. It is interesting to point out that the emission intensities of samples B and I are much stronger than those of samples D and J. This means the luminescent intensity in the $(ZnSe)(N_2H_4)_x(C_5H_5N)_y$ NSs is improved over that of the $(ZnSe)(C_5H_5N)_y$ NPs and that the intensity of ZnSe NSs is improved over that of ZnSe NPs.

4. Conclusions

In summary, inorganic–organic hybrid semiconductor $(ZnSe)(N_2H_4)_x(C_5H_5N)_y$ NSs as well as $(ZnSe)(C_5H_5N)_y$ NPs with different morphologies and compositions were successfully synthesized using a simple solvothermal method in a ternary solution. The morphologies and compositions of the products can be controlled by changing the reaction conditions. The photoluminescent properties of the composites were also studied. The results demonstrated that the morphologies and compositions of these hybrid semiconductors can influence the luminescent intensity of them.

Acknowledgements

This work was supported by High-Tech Research and Development Program of China (863) (Grant No. 2007AA03Z314), National Natural Science Foundation of China (Grant Nos. 10374086, 10504030 and 10704073) and Talent Youth Foundation of JiLin Province (Grant No. 20040105).

References

[1] A. Henglein, Chem. Rev. 89 (1989) 1861.
[2] S.T. He, J.N. Yao, S.J. Xie, H.J. Pang, Chem. Phys. Lett. 343 (2001) 28.
[3] A. Fukuoka, Y. Sakamoto, S. Guan, S. Inagaki, J. Am. Chem. Soc. 123 (2001) 3373.
[4] A.P. Alivisatos, Science, New Series 271 (1996) 933.
[5] H. Luo, J.K. Furdyna, Semicond. Sci. Technol. 10 (1995) 1041.
[6] Q. Peng, Y.J. Dong, Y.D. Li, Angew. Chem. Int. Ed. 42 (2003) 3027.
[7] S.B. Mirov, V.V. Fedorov, K. Graham, I.S. Moskalev, Opt. Lett. 27 (2002) 909.
[8] N. Kouklin, L. Menon, A.Z. Wong, D.W. Thompson, J.A. Woollam, P.F. Williams, Appl. Phys. Lett. 79 (2001) 4423.
[9] D.G. Shchukin, G.B. Sukhorukov, H. Mohwald, Angew. Chem. Int. Ed. 42 (2003) 4472.
[10] R.J. Chen, Y.G. Zhang, D.W. Wang, H.J. Dai, J. Am. Chem. Soc. 123 (2001) 3838.
[11] H. Zhang, Z. Cui, Y. Wang, K. Zhang, Adv. Mater. 15 (2003) 777.
[12] J. Jang, B. Lim, Angew. Chem. Int. Ed. 42 (2003) 5600.
[13] W.J. Li, X. Wang, Y.D. Li, Chem. Commun. (2004) 164.
[14] W. Yao, S.H. Yu, X.Y. Huang, J. Jiang, Adv. Mater. 17 (2005) 2799.
[15] X.Y. Huang, H.R. Heulings IV, V. Le, Chem. Mater. 13 (2001) 3754.
[16] D. Kaushik, M. Sharma, R.R. Singh, Mater. Lett. 60 (2006) 2994.
[17] S.L. Xiong, J.M. Shen, Y.Q. Gao, Q. Tang, Y.T. Qian, Adv. Funct. Mater. 15 (2005) 1787.
[18] Y.J. Dong, Q. Peng, Y.D. Li, Inorg. Chem. Commun. 7 (2004) 370.
[19] W.Z. Wang, Y. Geng, P. Yan, F.Y. Liu, Inorg. Chem. Commun. 2 (1999) 83.
[20] Z.X. Deng, L. Li, Y.D. Li, Inorg. Chem. 42 (2003) 2331.
[21] X.Y. Huang, J. Li, Y. Zhang, J. Am. Chem. Soc. 125 (2003) 7049.
[22] Z.X. Xiang, C. Wang, X.M. Sun, Y.D. Li, Inorg. Chem. 41 (2002) 869.
[23] Q. Peng, Y.J. Dong, Z.X. Deng, X.M. Sun, Y.D. Li, Inorg. Chem. 40 (2001) 3840.
[24] J.R. Durig, S.F. Bush, E.E. Mercer, J. Chem. Phys. 44 (1966) 4238.
[25] F.T. Quinlan, J. Kuther, W. Tremel, W. Knoll, S. Risbud, P. Stroeve, Langmuir 16 (2000) 4049.
[26] C.A. Smith, H.W.H. Lee, V.J. Leppert, S.H. Risbud, Appl. Phys. Lett. 75 (1999) 1688.
[27] A.B. Panda, S. Acharya, S. Efrima, Adv. Mater. 17 (2005) 2471.
[28] R. Lv, C.B. Cao, H.Z. Zhai, D.Z. Wang, S.Y. Liu, H.S. Zhu, Solid. State. Commun. 130 (2004) 241.
[29] C. Burda, X.B. Chen, R. Narayanan, M.A. El-sayed, Chem. Rev. 105 (2005) 1025.
[30] Y.D. Li, H.W. Liao, Y. Ding, Y. Fan, Y. Zhang, Y.T. Qian, Inorg. Chem. 38 (1999) 1382.
[31] Q.S. Wang, Z.D. Xu, Q.L. Nie, L.H. Yue, W.X. Chen, Y.F. Zheng, Solid. State. Commun. 130 (2004) 607.
[32] J. Yang, J.H. Zeng, S.H. Yu, L. Yang, G.E. Zhou, Y.T. Qian, Chem. Mater. 12 (2000) 3259.
[33] S.H. Yu, M. Yoshimura, Adv. Mater. 14 (2002) 296.
[34] G.T. Zhou, X.C. Wang, J.C. Yu, Cryst. Growth Des. 5 (2005) 1761.
[35] X.J. Chen, H.F. Xu, N.S. Xu, F.H. Zhao, W.J. Lin, G. Lin, Y.H. Fu, Z.L. Huang, H.Z. Wang, M.M. Wu, Inorg. Chem. 42 (2003) 3100.
[36] M.H. Chen, L. Gao, Mater. Chem. Phys. 91 (2005) 437.
[37] S. Fujita, H. Mimoto, T. Noguchi, J. Appl. Phys. 50 (1979) 1079.
[38] V. Ryzhikov, G. Tamulaitis, N. Starzhinskiy, J. Lumin. 101 (2003) 45.
[39] U. Philipose, S. Yang, T. Xu, E. Ruda, Appl. Phys. Lett. 90 (2007) 063103.